Journal of
Water & Climate Change

IWA PUBLISHING

Journal of Water and Climate Change Vol 15 No 8, 4099 doi: 10.2166/wcc.2024.269

Comparing the hybrid-lumped-LSTM model with a semi-distributed model for improved hydrological modeling

Erfan Zarei *, Farzin Nasiri Saleh and Afsaneh Nobakht Dalir

Department of Water Engineering, Faculty of Civil and Environmental Engineering, Tarbiat Modares University, Tehran, Iran
*Corresponding author. E-mail: erfanzarei@modares.ac.ir

EZ, 0000-0002-8160-7044

ABSTRACT

Accurate hydrological modeling is essential for understanding and managing water resources. This study conducts a comparative analysis of hydrological modeling strategies in a date-scarce region. This study examines lumped (IHACRES), semi-distributed (HEC-HMS), and hybrid-lumped/long short-term memory (LSTM) models, aiming to assess their performance and accuracy in a data-scarce region. It investigates whether lump models can accurately simulate flow and evaluates the impact of combining lump models with machine learning to enhance accuracy, compared to semi-distributed models. The IHACRES model underestimates discharge, but its commendable NSE during calibration (0.628) and validation (0.681) signifies reliable simulation. The HEC-HMS model accurately depicts daily streamflow but struggles with extreme events, showcasing limitations in predicting maximum flows. The hybrid-lumped/LSTM model exhibits improved accuracy over IHACRES. Despite some underestimation, it mitigates IHACRES limitations during extreme events. However, challenges persist in simulating high flows, emphasizing the necessity for further refinement. The findings contribute to the discourse on merging machine learning with traditional hydrological models in data-scarce regions. The hybrid model offers promise but underscores the need for ongoing research to optimize performance, especially during extreme events. This study provides valuable insights for advancing hydrological modeling capabilities in complex watersheds.

Key words: hybrid models, hydrological modeling, lumped models

HIGHLIGHTS

- Introducing a novel approach that combines traditional lumped models with Long Short-Term Memory (LSTM) machine learning for improved accuracy.
- Addressing challenges of modeling in data-scarce regions, demonstrating robust performance with minimal input data.
- Application of models in a complex watershed scenario, reflecting practical implications for water resource management.
- Comprehensive evaluation of lumped (IHACRES), semi-distributed (HEC-HMS), and hybrid lumped/LSTM models, highlighting their strengths and weaknesses.
- Integration of machine learning techniques to enhance the accuracy and reliability of hydrological models in challenging environmental conditions.

1. INTRODUCTION

Rapid urbanization, industrialization, and associated factors such as deforestation and land cover changes necessitate an accurate hydrological modeling to understand the evolving relationships between water dynamics and the environment across the various phases of the hydrological cycle (Devi *et al.* 2015). The main objective of hydrological modeling is to accurately replicate flows, aiming for minimal errors, and a proficient model is anticipated to demonstrate resilience to alterations in watershed conditions (Aqnouy *et al.* 2023). Hydrological models aid in decision-making, especially in situations with limited data and incomplete comprehension of a hydrological system (Duan *et al.* 2019; Ávila *et al.* 2022). Accurate hydrological modeling is crucial for effective water resource management and climate change adaptation, especially as populations increase and urbanization accelerates, making understanding water availability and flow dynamics increasingly important. Hydrological models not only aid in managing water resources but also play a vital role in predicting and mitigating the

impacts of climate change, such as altered precipitation patterns and more frequent extreme weather events (IPCC 2021). These models provide insights into how changes in land use, vegetation, and climate affect the water cycle, thereby assisting policymakers and water resource managers in making informed decisions (Bates *et al.* 2008).

Rainfall–runoff models can be categorized as either lumped or distributed models, depending on how the model parameters vary with spatial considerations (Devi *et al.* 2015). Lumped models consider the entire river basin as a single unit, disregarding spatial variability, while distributed models divide the catchment into small units to account for spatial variations in parameters and outputs (Moradkhani & Sorooshian 2008). In addition, machine learning models provide an efficient, data-driven approach with reduced data requirements and time demands compared to hydrological models (Mosavi *et al.* 2018; Wen & Feng 2023). Long-term short-term memory (LSTM) has gained significant popularity in machine learning competitions due to its speed, efficiency, and scalability and is used for different hydrological purposes such as flood susceptibility mapping (Fang *et al.* 2021), groundwater level prediction (Solgi *et al.* 2021), and water level prediction (Cho *et al.* 2022). LSTM has also been widely used for continuous runoff simulation in watersheds with abundant data availability (Ni *et al.* 2020; Xiang *et al.* 2020; Ren *et al.* 2022). Additionally, using machine learning models exclusively for streamflow simulation has drawbacks, including a tendency to neglect the physical aspects of the rainfall–runoff process (Mohammadi *et al.* 2022). Consequently, the fusion of hydrologic models and machine learning models has gained traction among hydrologists in recent years.

There has been recent research using lumped models such as the Hydrologiska Byråns Vattenbalansavdelning model (HBV), Identification of Hydrological Catchment Response and Simulation model (IHACRES), and semi-distributed model such as Hydrologic Engineering Center's Hydrologic Modeling System (HEC-HMS) for hydrological studies. For instance, Shakarneh *et al.* (2022) used HEC-HMS to simulate 20 rainfall–runoff events in two Palestinian catchments. The calibrated HEC-HMS model showed good performance for short-term flow forecasting in similar environments, aiding water resource managers in predicting and mitigating flood risks under future climatic scenarios. Esmaeili-Gisavandani *et al.* (2021) employed five hydrological models – Soil and Water Assessment Tool (SWAT), IHACRES, HBV, Australian Water Balance Model (AWBM), and Soil Moisture Accounting (SMA) – to simulate the Hablehroud River flow in north-central Iran. During calibration, SWAT, IHACRES, and HBV yielded satisfactory results. However, in the validation phase, only the SWAT model demonstrated excellent performance, surpassing the other models. Sorman *et al.* (2020) evaluated HEC-HMS and HBV-light for the water years from 2008 to 2015 in the mountainous headwaters of the Aras Basin in eastern Turkey. The findings indicated that HEC-HMS exhibited superior performance compared to HBV-light.

In poorly gauged areas, hydrological modeling becomes difficult, prompting researchers to employ various techniques to enhance model accuracy. For instance, (Rahman *et al.* 2020) utilized two merged precipitation datasets (MPDs) to predict daily streamflow using the SWAT in the Potohar Plateau, Pakistan. The study concludes that MPDs combine the strengths of individual satellite precipitation datasets and show greater potential for hydrological applications. Brocca *et al.* (2020) examined river flow prediction in regions with limited data, particularly focusing on West Africa. They discovered that incorporating satellite rainfall data with soil moisture measurements yielded more accurate predictions of river flow compared to relying solely on rain gauge observations. Akhtar *et al.* (2021) utilized remote sensing in conjunction with the SWAT to simulate the effects of climate change on water resources in the Kabul River Basin (KRB). They derived many of the biophysical parameters necessary for the SWAT model from remote sensing algorithms. Their findings suggest that integrating remote sensing data with the SWAT model can be a valuable approach to facilitate sustainable management and strategic planning of water resources in the KRB. Furthermore, many other studies used a combination of hydrological models and machine learning to increase the accuracy of their hydrological simulation. For example, Young & Liu (2015); Narayana Reddy & Pramada (2022) integrated HEC-HMS with an artificial neural network (ANN) to forecast runoff. Their developed hybrid model, HEC-HMS–ANN, showed improved accuracy in predicting runoff outcomes. Achite *et al.* (2022) applied the Modello Idrologico SemiDistribuito in continuo (MISD) model, a conceptual hydrological model, along with the group method of data handling to simulate daily streamflow in the Kalixälven River basin in northern Sweden. Their findings revealed that integrating meteorological variables into the existing conceptual hydrological model with parallel settings enhances the accuracy of streamflow simulation using deep learning models.

It is notable that our research explores the effectiveness of combining machine learning and traditional hydrological models, particularly in regions with limited data. Emphasizing the significance of our study being conducted in a data-scarce region, where hydrological modeling is particularly challenging due to the lack of extensive data, distinguishes our

research from studies conducted in more data-rich environments. This underscores the unique challenges faced in accurately modeling water dynamics. Our study provides a thorough assessment of model accuracy, incorporating both quantitative metrics and qualitative evaluations of each model's performance, especially during extreme events. While previous studies may have evaluated similar models, our research examines their performance specifically in the context of limited data availability, which affects model accuracy differently. Therefore, the objective of this study is to conduct a comparative analysis between lumped model and a combined lumped and LSTM model, requiring minimal input data (limited to precipitation and temperature), and a semi-distributed model. The primary focus is to address the inquiry of whether lump models can accurately simulate flow in a data-scarce region and evaluates the impact of combining lump models with machine learning to enhance accuracy, compared to semi-distributed models.

The following is how the rest of the text is organized. In Section 2, detailed information about the study area, including its geographical features and the dataset used, is provided. Section 3 discusses the specific hydrological models employed in our analysis, including lumped, semi-distributed, and hybrid models, outlining their methodologies and parameters. Moving forward, the results of our calibration and validation processes for each model are presented in Section 4, evaluating their performance in accurately simulating streamflow. This includes an in-depth discussion on the strengths and limitations of each model. Finally, in the conclusions section, insights into the implications of our findings for water resource management are provided, discussing how these models can assist in decision-making and adaptation strategies. The need for further research to improve the accuracy and applicability of hydrological models in addressing the challenges posed by urbanization and climate change is also highlighted.

2. MATERIALS AND METHODS

2.1. Study area and dataset

Located in the western part of Iran, the Kashkan watershed is a notable region renowned for its rivers. Over time, the presence of these rivers has led to the establishment of numerous settlements along the watercourses in the province. Covering an expansive area of 9,560 km^2, the Kashkan River exhibits an average annual discharge of 52 cubic meters per second, contributing to a total annual discharge volume of 1 billion and 636 million cubic meters. On April 1, 2019, the Kashkan River experienced an unprecedented event, with a peak flow recorded at approximately 5,232 cubic meters per second at the watershed's outlet. This extraordinary occurrence resulted in severe damage to a significant number of residential units, roads, agricultural lands, and critical infrastructure, causing substantial human and financial losses.

This study incorporates data consisting of daily cumulative precipitation values, daily maximum and minimum temperature data obtained from four synoptic stations, as well as daily cumulative precipitation values from 18 rain gauge stations and daily maximum discharge data from nine hydrometric stations. It is essential to underscore that all the data employed in this research, including meteorological data and land use maps, were sourced from reputable institutions such as the Iran Meteorological Organization and the Iran Water Resources Management Company. The geographic positioning of the study area, along with the strategic placement of hydrometeorological stations, is depicted in Figure 1.

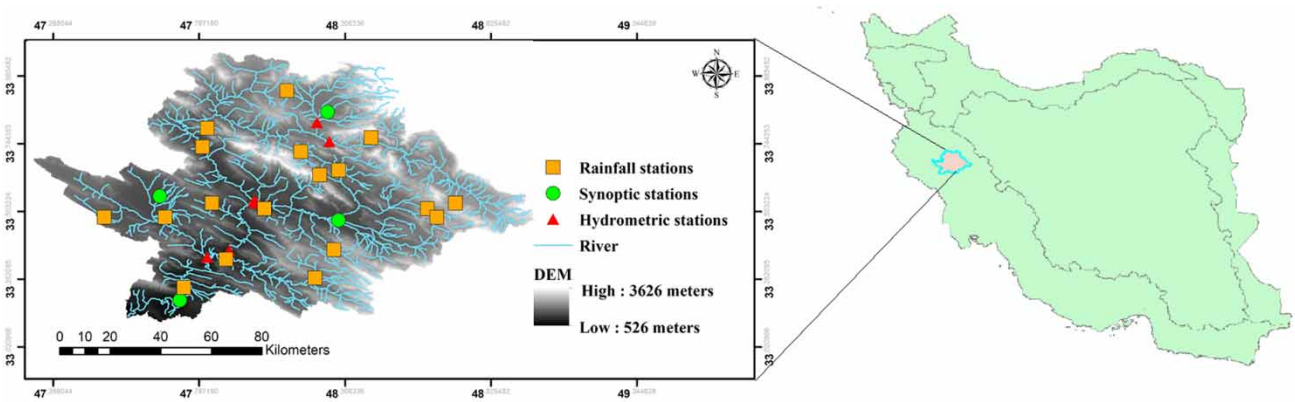

Figure 1 | Geographical location of the study area and location of hydrometeorological stations.

3. METHODOLOGY

3.1. Lump model

The IHACRES model is a lump model that can be used in different climatic regions, including arid and semi-arid regions (Croke & Jakeman 2008). The main purpose of the IHACRES model is to determine the hydrological behavior of the basin using a small number of parameters. This method consists of the nonlinear reduction module and the linear hydrograph module. The nonlinear module converts the rainfall (r_k) and temperature (t_k) to the effective rainfall (u_k) at each time step (k). Then, a linear relationship between rainfall (u_k) and flow (x_k) is assumed, and a unit hydrograph is generated. To estimate the amount of rainfall that will be effective, calculations are performed for both the basin moisture index and basin saturation index at each time step. Equations (1) and (2) correspond to the calculations for the effective rainfall (u_k) and SM index (φ_k), respectively (Carcano *et al.* 2008; Mohammadi *et al.* 2022):

$$u_k = [c(\phi_{\mathrm{k}} - l]^p \times r_k \tag{1}$$

$$\phi_k = r_k + \left(1 - \frac{1}{\tau_k}\right)\phi_{k-1} \tag{2}$$

The formula for runoff generation at a given time (k) is determined by a combination of two components: fast flow ($x_k^{(q)}$) and slow flow ($x_k^{(s)}$). This is influenced by various factors including the equilibrium coefficient of rainfall (c), drying rate (τ_k), SM index threshold (l), nonlinear response terms (p), and observed rainfall (r_k) (Mohammadi *et al.* 2022):

$$\mathrm{x}_k = x_k^{(q)} + x_k^{(s)} \tag{3}$$

$$x_k^{(q)} = -\alpha_q x_{k-1}^{(q)} + \beta_q u_k \tag{4}$$

$$x_k^{(s)} = -\alpha_s x_{k-1}^{(s)} + \beta_s u_k \tag{5}$$

$$\tau_q = \frac{-\Delta}{Ln(-\alpha_q)} \tag{6}$$

$$\tau_s = \frac{-\Delta}{Ln(-\alpha_s)} \tag{7}$$

$$v_{\mathrm{q}} = 1 - v_s = 1 - \frac{\beta_s}{1 + \alpha_s} \tag{8}$$

α_q and β_q represent fixed time parameters for fast flow, while α_s and β_s represent fixed time parameters for slow flow. Δ indicates a time period, τ_q and τ_s denote fixed time periods for fast and slow daily flows, respectively. v_q is the proportion of fast flow to overall flow ($1 - v_s$), and v_s indicates the proportion of slow flow (Abushandi & Merkel 2013; Mohammadi *et al.* 2022).

3.2. Hybrid model (IHACRES/LSTM)

The LSTM, or long short-term memory, network represents a specialized form of recurrent neural network (RNN) designed to address the challenge of long-term memory retention in standard RNNs (Olah 2015). Unique to the LSTM architecture are internal mechanisms known as gates, which regulate the information flow within the cells. The sigmoid function is integral to this process, facilitating the forgetting of the prior cell state as the layer-generated value approaches zero. Key components of the LSTM model include the forget gate (f_t), the input gate (i_t), and the output gate (h_t).The input gate, employing the sigmoid function (σ), plays a crucial role in determining the update of existing information. Equations (9)–(11) illustrate the functioning of the input gate (i_t), where W and b denote the weights and biases within each LSTM cell, x_t represents the input, and h_{t-1} is the previous result. The candidate for new cell state values, denoted as C′ (Xiang *et al.* 2022), is calculated using a

hyperbolic tangent (tanh) function. C_t signifies the current cell state, while C_{t-1} represents the previous cell state:

$$i_t = \sigma(W_i \cdot [h_{t-1}] + b_i) \tag{9}$$

$$C'_t = \tanh(W_C \cdot [h_{t-1}.x_t] + b_c \tag{10}$$

$$C_t = f_t \times C_{t-1} + i_t \times C'_t \tag{11}$$

Equation (12) outlines the role of the forget gate (f_t), specifying its function in determining the significance of data within the sequence that should be retained and identifying data that should be discarded.

$$f_t = \sigma(W_f \cdot [h_{t-1}.x_t] + b_f) \tag{12}$$

The final stage of extracting valuable information from the entire structure and presenting it as output data is overseen by the output gate (Tasabat & Aydın 2021). The functionality of the output gate (h_t) is elucidated in Equations (13) and (14), where h_t results from the multiplication of o_t and the hyperbolic tangent function value of the cell state C_t (Xiang *et al.* 2022):

$$o_t = \sigma(W_o \cdot [h_{t-1}.x_t] + b_o \tag{13}$$

$$h_t = o_t \times \tanh(C_t) \tag{14}$$

The complexities of the LSTM models are depicted in Figure 2. Furthermore, the GridSearchCV technique was employed to determine the optimal combination of hyper parameters for the LSTM model.

An essential phase in preparing input variables for a machine learning model involves screening potential factors, coupled with the runoff output generated by IHACRES. Commonly considered variables include rainfall, maximum temperature, minimum temperature, and evapotranspiration. In alignment with the study's goals and the data accessibility in the region, this research integrates precipitation and average temperature, along with the predicted runoff output from IHACRES.

3.3. HEC-HMS model

The HEC-HMS model, first introduced in 1968 by the US Army Engineering Hydrology Center, falls into the category of semi-distributed, computer mathematical models employed to simulate watershed reactions to rainfall events, including surface flow and flood dynamics (Yu & Zhang 2023). In a specific area, the HEC-HMS requires three main components: the basin model, meteorological model, and time series data (Oleyiblo & Li 2010). To create the basin model, we obtained the SRTM digital elevation map from https://earthexplorer.usgs.gov/ for the watershed. Using this map, we calculated the accumulation map and flow direction. Following this, the watershed was divided into 15 sub-basins, as illustrated in Figure 3, taking into account factors such as land use maps, basin slope, and the presence of hydrometric stations.

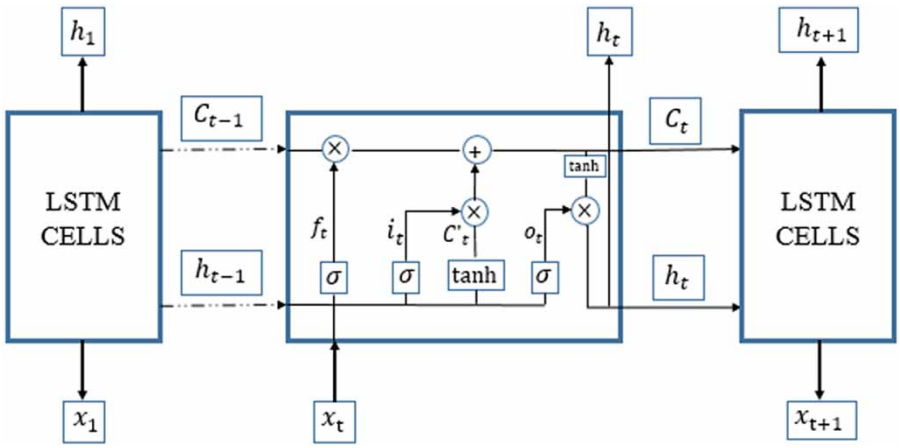

Figure 2 | The architecture of the LSTM network.

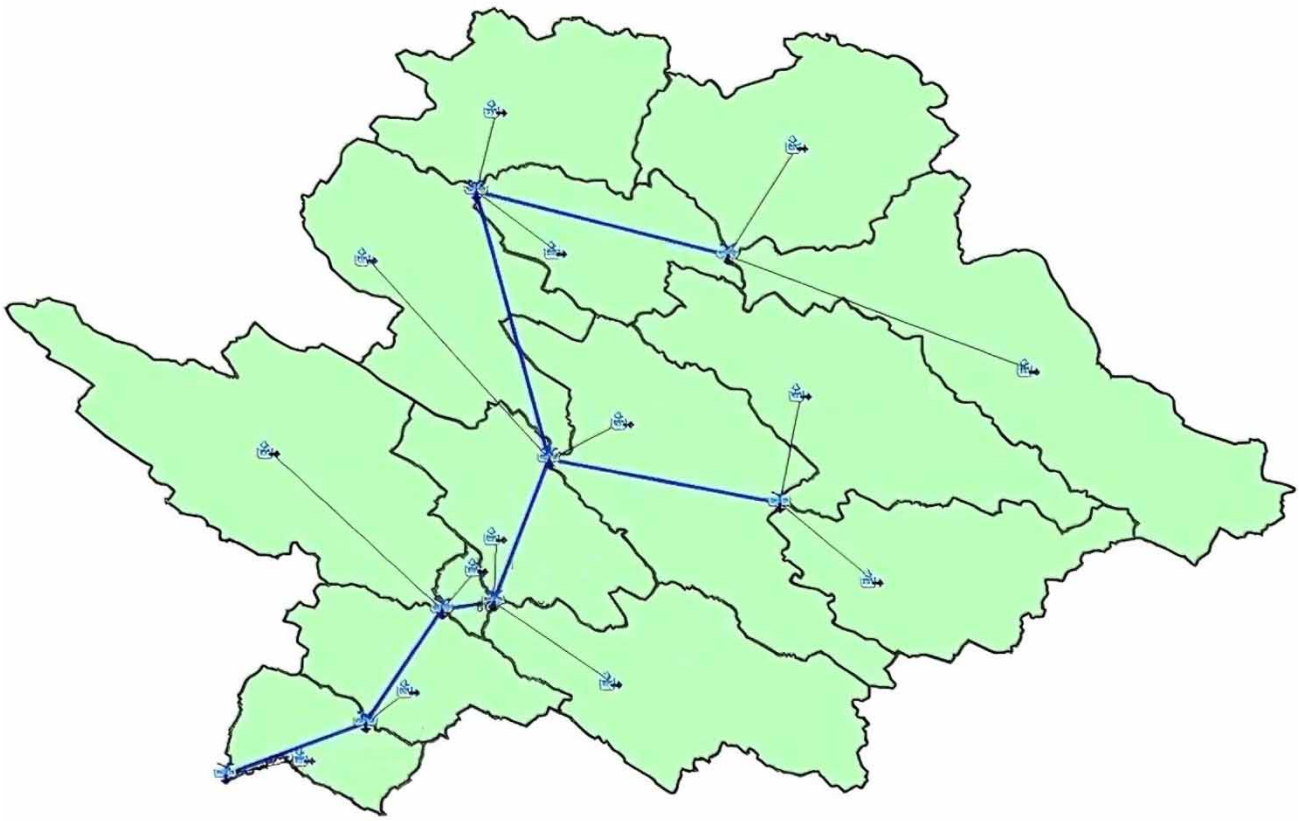

Figure 3 | Basin model setup in HEC-HMS.

3.3.1. Basin model

3.3.1.1. Canopy (simple canopy). The sub-basin incorporates a canopy component designed to simulate the vegetation in the region, employing the HEC-HMS canopy method primarily for continuous simulations, where rainfall accumulates until the canopy storage capacity is reached (Ouédraogo *et al.* 2018). This method requires two parameters: initial storage in percentage and maximum storage in millimeters. Assuming zero initial storage (dry leaves and tree trunks at the beginning of modeling), calculation of evaporation and transpiration in dry and wet period and simple absorption method, initial values of maximum storage were calculated from the land use map and the coefficients suggested by USACE.

3.3.1.2. Surface (simple surface). This method offers a simple representation of the top layer of soil, where rainfall accumulates until reaching the surface's maximum capacity. Infiltration is possible even before reaching full capacity, but if precipitation exceeds the infiltration rate, surface runoff occurs. This method requires two parameters: initial storage in percentage and maximum storage in millimeters. We assume that in the start of our model all the lands are dry (initial storage = 0) and we estimated the maximum storage based on the slope, more detail can be found in Fleming & Neary (2004).

3.3.1.3. Routing (Muskingum method). The Muskingum method, an essential tool in hydrological modeling for simulating water flow through river networks, offers valuable insights into flood routing, reservoir operations, and water resources management (Chow 1998). This method, a widely used lumped flow routing technique, involves calibrating two parameters, X and K (Hamdan *et al.* 2021). X, a dimensionless weight ranging from 0 to 0.5, signifies the relative impact of flow on storage levels (Hamdan *et al.* 2021). Initially set at 0.1, X is adjusted during calibration. K, a time-related parameter (in hours) ranging from 1 to 5, is associated with the delay between discharge peaks (Din *et al.* 2019). Equation

(15) is utilized to estimate the value of K:

$$K = \frac{L}{V_w} \tag{15}$$

The flood wave velocity (V_w), considered as 1.5 times the average velocity, and the reach length (L) are calculated using data obtained from stream gauging sites (Hamdan *et al.* 2021).

3.3.1.4. Loss (SMA). The SMA accurately represents soil moisture dynamics within the watershed, capturing spatial and temporal variations under different climatic conditions. It integrates multiple factors including soil properties, land cover, and climate data, providing a comprehensive understanding of soil moisture influences. Additionally, its flexibility allows adaptation to different geographic areas and land use scenarios, making it versatile for various applications. The methods' utility extends to water resources management, aiding in water availability assessment, runoff prediction, and decision-making. The SMA method replicates the flow and retention of water within the soil profile and across various groundwater layers (Leavesley *et al.* 1983). The upper threshold for the rate at which water enters the soil from surface storage, known as the maximum infiltration rate, was established by analyzing the soil in the catchment, reflecting the saturated hydraulic conductivity (Saxton & Willey 2005). The impervious area was identified as the percentage of the urban area, and these values were calculated based on a land use/land cover map. The determination of storage coefficients and depths for GW1 and GW2 relied on an analysis of historical flow data related to streamflow recession (Ouédraogo *et al.* 2018) The average hydraulic conductivity of all sub-basins was selected as the percolation rate for both soil and the first groundwater layer (GW1) (Ouédraogo *et al.* 2018). The starting values for soil water storage, defined as porosity, tension storage representing the field capacity of the soil, and the percolation rate of GW2 were sourced from the Davtalab *et al.* (2017) study, where they incorporated the Kashkan watershed as one of their sub-basins.

3.3.1.5. Base flow (recession). The recession base flow technique aims to mimic the common patterns observed in watersheds as channel flow gradually diminishes in an exponential manner. Due to varying water withdrawals in the main stream and sub-basin rivers, the base flow of the Kashkan watershed exhibits nonlinear behavior, making recession the most suitable method for simulating base flow in this study. The starting base flow (in cubic meters per second) needs to be defined at the start of a simulation. The recession constant indicates the pace at which base flow diminishes between storm events, and by using the parameter of the ratio to peak, we can determine the approach for resetting the base flow during storm events. Those parameters were estimated by analysis of historical flow data.

3.3.1.6. Transform (Clark unit hydrograph). Among the options to convert the calculated rainfall excess, derived from the rainfall loss computation, into direct runoff for sub-basin continuous modeling that requires less hydrological data related to the characteristics of the watershed, two commonly used methods are the Clark unit hydrograph and the SCS (Soil Conservation Service) unit hydrograph. The Clark unit hydrograph is particularly suitable for small watersheds (Subramanya 2008), making it a preferred choice due to its higher accuracy in such conditions. The Clark unit hydrograph necessitates the determination of time of concentration and storage coefficient (Chiang *et al.* 2022). The time of concentration (T_c) in hours can be approximated using Kirpich's formula, taking into account basin characteristics such as topography and reach length (Kirpich 1940):

$$T_c = 0.0078 \times \left(\frac{L^{0.77}}{S^{0.385}} \right) \tag{16}$$

where L is the reach length in kilometers, and S is the slope in (meter/meter). Storage coefficient (R) values can be calculated from Equation 17 (Sabol 1988), where in this equation A is the catchment area in (km^2):

$$\frac{T_c}{\mathrm{R}} = \frac{146}{100} - \frac{0.0867L^2}{A} \tag{17}$$

3.3.2. Metrological model

The Thieesen weight method was used to assign precipitation in each sub basin. This approach allocates a designated region, termed a Thiessen polygon, to each gauge, where the Thiessen polygon represents the area where any randomly chosen point within it is closer to the specific gauge than to any other gauge. Due to the absence of shortwave radiation time series data the Hamon method was employed for estimating evapotranspiration. The calculation involves determining the average potential evapotranspiration (ET_o) as outlined by Hamon (1963):

$$ET_o = c\frac{N}{11}P_t \tag{18}$$

Here, c represents a coefficient, N denotes the count of daylight hours, and P_t stands for the saturated water vapor density at the daily mean temperature. According to the HEC-HMS User Manual (U.S. Army Corps of Engineers 2018), the only input for this method in HEC-HMS is the coefficient (mm/g/m^3), where the initial value is 0.1651 mm/g/m^3, then it was calibrated during the calibration process.

Due to lack of snow water equivalent time series, temperature index method was used for snow modeling. In this degree-day approach a fixed amount of snowmelt for each degree above freezing is considered. The parameters for these methods are: lapse rate which represents the temperature change per 1,000 m, it is typically −6.5 °C (Muralikrishna & Manickam 2017). The PX temperature is employed to differentiate between rain and snow, with any precipitation occurring when the air temperature is below the specified threshold assumed to be snow, according to field surveys this value is equal to 1.5 °C. The base temperature in set to be 0, that means if the air temperature is less than the base temperature, then the amount of melt is zero. Another parameter is wet melt rate (millimeter/degree °C-day) and dry melt rate (millimeter/degree °C-day), where the initial values were selected from Davtalab *et al.* (2017) then calibrated.

3.4. Model evaluation

To calibrate the models, the time frame considered spanned from January 1, 1997, to December 31, 2012. Validation, on the other hand, involved the period from January 1, 2013, to August 31, 2019. Evaluation metrics, including the coefficient of determination (R^2), Nash-Sutcliffe Efficiency (NSE), and the average error in peak flow (AEPF) for annual maximum flow, were utilized to comprehensively assess model accuracy during both calibration and validation phases (as indicated by the following equations):

$$R^2 = \left[\frac{\sum_{i=1}^{n}(QO_i - QO_m) \times (QS_i - QS_m)}{\sqrt{\sum_{i=1}^{n}(QO_i - QO_m)^2 \times \sum_{i=1}^{n}(QS_i - QS_m)^2}}\right] \tag{19}$$

$$\mathrm{NSE} = 1 - \left[\frac{\sum_{i=1}^{n}(QO_i - QS_i)^2}{\sum_{i=1}^{n}(QO_i - QO_m)^2}\right] \tag{20}$$

$$\mathrm{AEPF} = 100 \times \frac{\left(\sum_{i=1}^{N}|QPO_i - QPS_i|/QPO_i\right)}{N} \tag{21}$$

Here, QO and QS denote observed and simulated flow rates, respectively. QPO and QPS represent the maximum flow rates for each hydrograph. QO_m stands for the mean observed flow, and N is the count of computed hydrograph ordinates. All flow values are expressed in cubic meters per second (m³/s). A model is deemed superior as the R^2 and NSE values approach 1, and a lower AEPF value approaching 0 signifies enhanced performance.

4. RESULTS AND DISCUSSION

4.1. Models calibration and validation

4.1.1. HEC-HMS model

For calibration purposes, we utilized the inherent calibration functions in the software, which include Percentage Bias and Peak Weighted RMSE. Additionally, considering the multitude of parameters in HEC-HMS and drawing insights from previous research (Fleming & Neary 2004; Bhuiyan *et al.* 2017; Dariane *et al.* 2019), we also incorporated a manual calibration approach. This involved calibrating the discharge for each hydrometric station from the upper sub-basins to the outlet for the calibration period. Table 1 illustrates the parameter value ranges employed for sub-basins throughout the calibration process.

During both the calibration and validation periods, HEC-HMS accurately replicated the hydrograph at the basin outlet, as illustrated in Figure 4, showcasing its precise depiction of notable variations in daily streamflow. However, concerning the simulation of maximum flow, there are instances of underestimation. For example, on April 1, 2019, there was a peak flow of 5,237 m^3/s, which caused significant human and financial losses. However, our model predicted this peak flow to be 3,396.16 m^3/s, showing a considerable difference. Also, the model consistently overestimates the base flow of the basin, mainly because of increased groundwater withdrawals in the surrounding area. In dry seasons, when river flow hits its lowest points, we often see overestimation in HEC-HMS simulation. For example, in 2017, a particularly dry year for the region, the summer season saw an average observed flow of 7.1 m^3/s, while the simulation showed a higher value of 10.8 m^3/s.

Table 2 presents an evaluation of the model's performance using three distinct metrics. Specifically, the values for R^2, NSE, and $AEPF1_y$ were 0.859, 0.696, and 15.21%, respectively. In the validation phase, these values were 0.916, 0.831, and 23.62%. Additionally, the $AEPF1_y$ for HEC-HMS was 15.21% during calibration and 23.62% during validation, indicating a notable discrepancy and underscoring the model's limitations in accurately simulating high flows.

Table 1 | The range of parameter values pertaining to the sub-basins during the calibration process

Sub-models	Parameters	Definition	Range for calibrated values
Canopy method	Max storage (mm)	Amount of water that can be held on leaves	1–1.70
Surface storage	Max storage (mm)	Amount of water that can be held on the soil surface	10–25
Loss method	Max infiltration	Upper bond on infiltration from the surface to the soil	0.8–1.2
	Impervious	Land surface that does not allow water to infiltrate	8–20
	Soil storage	Total storage availabe on the soil	40–120
	Tension storage	Quantity of water that remains stationary	10–30
	Soil precolation	Upper bound on precolation from the soil storage into the upper ground water	10–30
	GW1 storage	Total storage in the upper ground water layer	20–80
	GW1 precolation	Percolation from the upper groundwater into the lower groundwater	0.05–10
	GW1 coefficient	Delay in transforming stored water to lateral outflow in a linear reservoir	150–800
	GW2 storage	Total storage in the lower growndwater	2–40
	GW2 precolation	Upper bound on deep precolation out of the system	1–10
	GW2 coefficient	Delay in transforming stored water to lateral outflow in a linear reservoir	250–900
Transform	Time of concentration	Maximun travel time in the sub-basin	10–80
	Storage coefficient	Accounts for storage effects	25–100
Baseflow	Recession constant	Rate at which baseflow receds between storm events	0.85–0.995
	Ratio	Proportion of groundwater discharge that is attributed to baseflow	0.03–0.30
Evaportranspiration	Hamon coeficient	Used to estimate potential evapotranspiration	0.10–0.16
Snowmelt	PX temperature	Discriminate between precipitatiom falling as rain or snow	1–1.5
	Wet meltrate	The rate at which snowpack melts when it is raining	1–4.5
	Dry meltrate	The rate at which snowpack melts when it is no raining	1–4.5

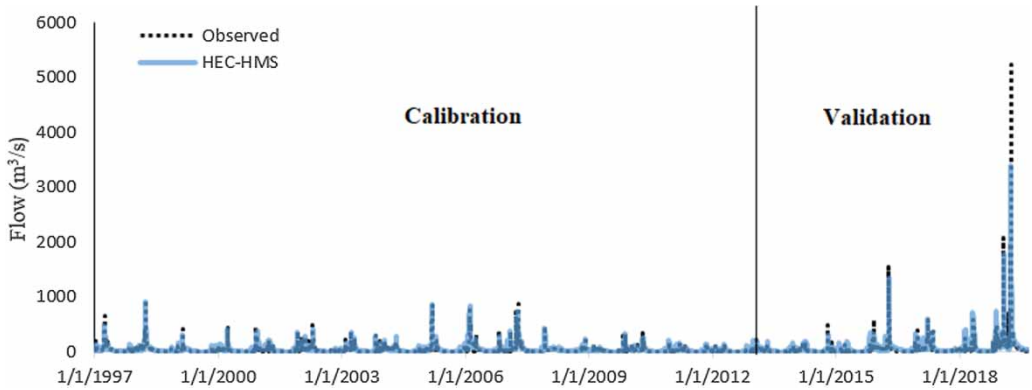

Figure 4 | Hydrograph simulated by HEC-HMS.

Table 2 | Accuracy assessment of HEC-HMS

Model	Period	R^2	NSE	$AEPF_{1y}$ (%)
HEC-HMS	Calibration	0.859	0.696	15.21
	Validation	0.916	0.831	23.62

4.1.2. IHACRES

The IHACRES hydrological model was employed to conduct hydrological modeling in this study. For the calibration of IHACRES models, a grid search function was utilized, which is originally implemented in the IHACRES 2.1.2 software. In this calibration section, a range for each parameter can be identified. The calibrated values of IHACRES are presented in Table 3, providing detailed insight into the calibration process and its outcomes.

In Figure 4, the hydrograph produced by the IHACRES model is presented. Throughout the entire duration from 1997 to 2019, the IHACRES model consistently underestimates the discharge in comparison to the observed data. Notably, during the validation period from January 1, 2013, to August 31, 2019, the underestimation is more prominent. Specifically, during the flood event on April 1, 2019, where the observed data records a flow of 5,237 m^3/s, IHACRES generates a lower flow of 3,978 m^3/s. For the IHACRES model, although overestimation persists in flow simulation during dry seasons, the error tends to be lower compared to the HEC-HMS model. For instance, in the summer of 2017, the average observed flow was 7.1 m^3/s, while the simulation showed a slightly higher value of 8.7 m^3/s.

Table 4 offers a comprehensive assessment of the IHACRES model's performance across two distinct periods, employing three key metrics. The NSE indicates commendable performance during both calibration (0.795) and validation (0.826), with the latter period showing a slight improvement. The $AEPF1_y$ values of 43.63% and 56.59% during calibration and validation,

Table 3 | The optimal values during the calibration process for the IHACRES model

Parameters	Description	Optimal value
τ_q	Time constant governing the rate of recession of quick flow (day)	8.229
τ_s	Time constant governing rate of recession of slow flow (day)	278.933
v_s	The proportion of slow flow to total flow (proportion)	0.294
t_w	Drying rate at reference temperature (day)	7
f	Temperature dependence of drying rate ($°C^{-1}$)	4
C	Mass balance term (mm)	0.0015

Table 4 | Accuracy assessment of the IHACRES model

Model	Period	R^2	NSE	$AEPF_{1y}$ (%)
IHACRES	Calibration	0.795	0.628	43.63
	Validation	0.826	0.681	56.59

respectively, highlight the model's incapability in modeling high flows, which can contribute to the higher error in observation data in extreme whether event.

4.1.3. Hybrid model

As an input to the LSTM model for generating hybrid model, output runoff from IHACRES, daily precipitation, and average temperature were used. Grid search was utilized to find the best parameters for LSTM, calibrated parameters are outlined on Table 5.

Figure 5 shows the runoff output generated by the hybrid model. While there are still some noticeable underestimations, the overall magnitude of underestimation has decreased.. For example, on April 1, 2019, the hybrid model yielded a value of 4,785 m^3/s, which represents an improvement compared to the IHACRES-generated value of 3,978 m^3/s. For the hybrid model, during the dry summer season of 2017, the average observed flow was 7.1 m^3/s, while the simulation indicated 8.21 m^3/s. This suggests that combining the two models slightly improves the performance of the IHACRES model in low flow simulation.

Table 6 displays the accuracy assessment metrics for the hybrid model. During the calibration period, all metrics showed slight improvements, but these were more substantial during the validation period. However, there was not a significant improvement in handling high flows, highlighting the hybrid model's inadequacy in simulating maximum flows.

Table 5 | The optimal values and states during the calibration process for the LSTM model

Parameters	Optimal value/state
Number of layers	2
Number of neurons in the first layer	150
Number of neurons in the second layer	100
Activation function	Relu
Optimizer	Adam
Loss	MSE
Epochs	200
Batch size	10

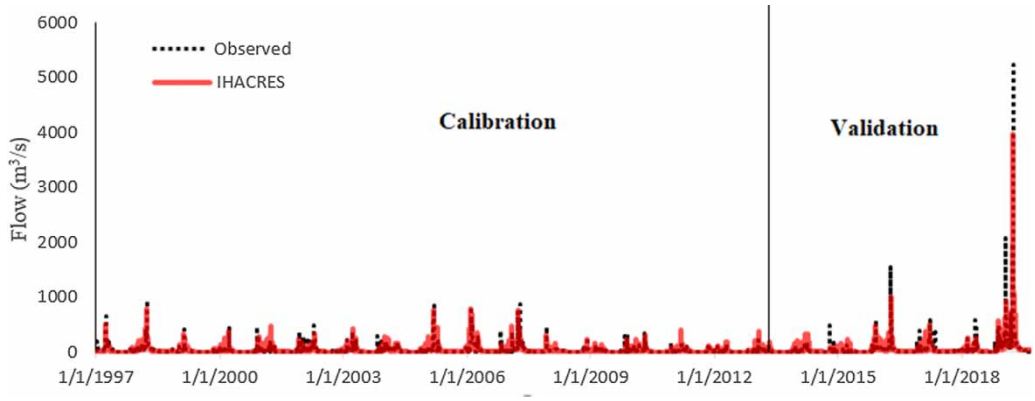

Figure 5 | Hydrograph simulated by the hybrid model.

Table 6 | Accuracy assessment of the hybrid model

Model	Period	R^2	NSE	$AEPF_{1y}$ (%)
Hybrid model	Calibration	0.803	0.644	38.70
	Validation	0.955	0.909	45.23

5. CONCLUSION

This study undertook a comparative analysis between a hybrid-lumped and LSTM model, requiring minimal input data, and a semi-distributed model for hydrological modeling in the Kashkan watershed in western Iran. The research aimed to address the question of whether the hybrid-lumped/LSTM model could achieve comparable accuracy to a semi-distributed model, which requires a more extensive dataset.

The lumped model IHACRES, the semi-distributed model HEC-HMS, and the hybrid-lumped/LSTM model were calibrated and validated using various hydrological metrics. The HEC-HMS model exhibited accurate simulation of daily streamflow but showed limitations in accurately predicting high flows, particularly during extreme events such as the flood on April 1, 2019. The IHACRES model, while underestimating discharge, displayed inaccurate performance, especially in simulating high flows.

The hybrid-lumped/LSTM model, incorporating machine learning techniques, demonstrated improved accuracy compared to IHACRES, particularly in the validation phase. The model addressed some of the limitations of IHACRES, reducing the underestimation of discharge, especially during extreme events. However, challenges remain in accurately simulating high flows, emphasizing the need for further refinement and exploration of hybrid modeling approaches.

In comparing our study with similar hydrological modeling research conducted in neighboring countries or regions, several trends and differences emerge. For instance, Prakasam *et al.* (2023) investigated hydrological modeling in Himalayan catchment, utilizing the HEC-HMS model, which showed satisfactory performance in simulating daily streamflow, while our study also achieved accurate daily streamflow simulation using the HEC-HMS model. Esmaeili-Gisavandani *et al.* (2021) focused on hydrological modeling in the Hablehroud River, north-central Iran, employing various models including IHACRES and HBV-light, both of which demonstrated good performance in simulating streamflow. However, both our study and Esmaeili-Gisavandani *et al.* (2021) identified challenges in accurately predicting high-flow events. Garee *et al.* (2017) found limitations in the SWAT model's ability to accurately simulate high flows. They conducted a case study in the Glacierized Catchment Hunza and observed consistent underestimation of discharge by the SWAT model, particularly during high-flow events. Sorman *et al.* (2020) studied the hydrological modeling of the upper Aras Basin, Turkey, using HBV-light and also encountered challenges in modeling high flows. In the study conducted by Narayana Reddy & Pramada (2022), which utilized a combination of HEC-HMS and ANN for flow simulation in an Indian watershed, the underestimation of the hybrid model during extreme high flows was also observed in their study, aligning with our findings. In summary, employing lumped models for hydrological modeling in data-scarce regions can result in inaccuracies in high-flow modeling. Despite the use of hybrid models improving the overall performance of hydrological models, the issue of inaccuracies in simulating high flows may persist. These comparisons highlight commonalities in modeling approaches, such as the use of meteorological and topographic data, but also underscore differences in model performance, particularly in capturing extreme precipitation events. By understanding these trends, our study contributes to the broader understanding of hydrological dynamics in the region and emphasizes the need for improved modeling approaches to support water resource management.

Discussing the limitations of hydrological models such as HEC-HMS, HBV-light, and hybrid models requires considering various aspects of their structure, assumptions, and application. HEC-HMS poses several limitations, including its complexity in setup, necessitating detailed input data on topography, land use, soil properties, and meteorological data, which may not always be available or precise. Its accuracy heavily relies on parameterization, and poorly calibrated parameters can result in significant discrepancies between simulated and observed hydrographs. Additionally, its spatial and temporal resolution might not adequately capture small-scale variability or short-duration events, potentially leading to underestimation or overestimation of runoff. Errors in precipitation input, parameter uncertainties, and simplifications in the model structure further contribute to potential sources of error or uncertainty. Similarly, HBV-light simplifies hydrological processes such as snowmelt and soil moisture dynamics, which may not fully represent real-world conditions, especially in complex terrain or areas with non-uniform land cover. Its simple linear reservoir approach for channel routing may also not accurately capture the

dynamics of fast-flowing events or flood routing. Errors can arise from inaccuracies in snowmelt estimation, soil moisture dynamics, and uncertainties in parameter values, particularly in regions with limited observational data. The hybrid model combining HBV-light and LSTM introduces complexity in model interpretation due to the interaction between the components and requires careful calibration and validation of both parts. Errors may emerge from the integration of HBV-light and LSTM components, inconsistent outputs, and limited transferability of LSTM models across different hydrological conditions and regions. Additionally, errors in input data quality, such as biases in meteorological data or inaccuracies in historical hydrological records, can affect the hybrid model's performance.

The findings of this study contribute to the ongoing discourse on the integration of machine learning techniques with traditional hydrological models. While the hybrid-lumped/LSTM model showed promise in enhancing the accuracy of hydrological simulations, further research is warranted to optimize the model's performance, especially in capturing extreme events. This study underscores the importance of considering both lumped and semi-distributed approaches, along with machine learning techniques, to advance hydrological modeling capabilities and improve decision-making in water resource management.

Overall, while the hybrid model offered some improvement over the individual models, all three models faced challenges in accurately simulating high-flow events. This highlights the limitations of these models in capturing the complex dynamics of watersheds susceptible to extreme weather events.

Future research directions:

- Explore alternative modeling approaches, such as fully distributed models, that can incorporate additional spatial and physical characteristics of the watershed.
- Investigate the integration of data assimilation techniques to improve model performance during high-flow events.
- Employ more advanced machine learning models or hybrid approaches, potentially incorporating additional relevant data sources (e.g., remote sensing data) to enhance model accuracy.
- Utilize more sophisticated optimization techniques, like meta heuristic approaches, in hybrid and machine learning models to enhance result accuracy.

By addressing these limitations and exploring new avenues, future research can contribute to the development of more robust and reliable hydrological models for accurate streamflow simulation, particularly in watersheds prone to extreme weather events.

ACKNOWLEDGEMENT

We appreciate the Iran Meteorological Organization for providing the data in this study.

DATA AVAILABILITY STATEMENT

Data cannot be made publicly available; readers should contact the corresponding author for details.

CONFLICT OF INTEREST

The authors declare there is no conflict.

REFERENCES

Abushandi, E. & Merkel, B. 2013 Modelling rainfall runoff relations using HEC-HMS and IHACRES for a single rain event in an arid region of Jordan. *Water Resources Management* **27**, 2391–2409.

Achite, M., Mohammadi, B., Jehanzaib, M., Elshaboury, N., Pham, Q. B. & Duan, Z. 2022 Enhancing rainfall-runoff simulation via meteorological variables and a deep-conceptual learning-based framework. *Atmosphere* **13**, 1688. https://doi.org/10.3390/atmos13101688.

Akhtar, F., Awan, U. K., Borgemeister, C. & Tischbein, B. 2021 Coupling remote sensing and hydrological model for evaluating the impacts of climate change on streamflow in data-scarce environment. *Sustainability* **13** (24), 14025. https://doi.org/10.3390/su132414025.

Aqnouy, M., Ahmed, M., Ayele, G. T., Bouizrou, I., Bouadila, A. & Stitou El Messari, J. E. 2023 Comparison of hydrological platforms in assessing rainfall-runoff behavior in a mediterranean watershed of Northern Morocco. *Water* **15**, 447. https://doi.org/10.3390/w15030447.

Ávila, L., Silveira, R., Campos, A., Rogiski, N., Gonçalves, J., Scortegagna, A., Freita, C., Aver, C. & Fan, F. Comparative evaluation of five hydrological models in a large-scale and tropical river basin. *Water* 2022, **14**, 3013. https://doi.org/10.3390/w14193013.

Bates, B. C., Kundzewicz, Z. W., Wu, S. & Palutikof, J. P. 2008 *Climate Change and Water. Technical Paper of the Intergovernmental Panel on Climate Change*. IPCC Secretariat, Geneva, 210 pp.

Bhuiyan, H. A. K. M., McNairn, H., Powers, J. & Merzouki, A. 2017 Application of HEC-HMS in a cold region watershed and use of RADARSAT-2 soil moisture in initializing the model. *Hydrology* **4** (1), 9. https://doi.org/10.3390/hydrology4010009.

Brocca, L., Massari, C., Pellarin, T., Filippucci, P., Ciabatta, L., Camici, S., Kerr, Y. H. & Fernández-Prieto, D. 2020 River flow prediction in data scarce regions: Soil moisture integrated satellite rainfall products outperform rain gauge observations in West Africa. *Scientific Reports* **10**, 12517. https://doi.org/10.1038/s41598-020-69343-x.

Carcano, E. C., Bartolini, P., Muselli, M. & Piroddi, L. 2008 Jordan recurrent neural network versus IHACRES in modelling daily streamflows. *Journal of Hydrology* **362**, 291–307.

Chiang, S., Chang, C.-H. & Chen, W.-B. 2022 Comparison of rainfall-runoff simulation between support vector regression and HEC-HMS for a rural Watershed in Taiwan. *Water* **14**, 191. https://doi.org/10.3390/w14020191.

Cho, M., Kim, C., Jung, K. & Jung, H. 2022 Water level prediction model applying a Long Short-Term Memory (LSTM)–Gated Recurrent Unit (GRU) method for flood prediction. *Water* **14**, 2221. https://doi.org/10.3390/w14142221.

Chow, V. T. 1998 *Open-Channel Hydraulics*, 2nd edn.. McGraw-Hill, New York.

Croke, B. F. & Jakeman, A. J. 2008 Use of the IHACRES rainfall-runoff model in arid and semiarid regions. In: *Hydrological Modelling in Arid and Semi-Arid Areas* (Wheater, H. S., Sorooshian, S. & Sharma, K. D., eds). Cambridge University Press, Cambridge, UK, pp. 41–48.

Dariane, A. B., Bagheri, R., Karami, F. & Javadianzadeh, M. M. 2019 Developing heuristic multi-criteria auto-calibration method for continuous HEC-HMS in snow-affected catchment. *International Journal of River Basin Management* **18** (1). 69–80. https://doi.org/10.1080/15715124.2019.1576696.

Davtalab, R., Mirchi, A., Khatami, S., Gyawali, R., Massah, A., Farajzadeh, M. & Madani, K. 2017 Improving continuous hydrologic modeling of data-poor river basins using hydrologic engineering center's hydrologic modeling system: Case study of Karkheh River Basin. *Journal of Hydrologic Engineering* **22** (8). https://doi.org/10.1061/(ASCE)HE.1943-5584.000152.

Devi, G. K., Ganasri, B. P. & Dwarakish, G. S. 2015 A review on hydrological models. *Aquatic Procedia* **4**, 1001–1007. doi:10.1016/j.aqpro.2015.02.126.

Din, S. U., Khan, N. M., Israr, M., Nabi, H. & Khan, M. 2019 Runoff modelling using HEC HMS for rural watershed. *Development* **6**, 79–85.

Duan, Q., Pappenberger, F., Wood, A., Cloke, H. L. & Schaake, J. 2019 *Handbook of Hydrometeorological Ensemble Forecasting*. Springer, Berlin/Heidelberg, Germany.

Esmaeili-Gisavandani, H., Lotfirad, M., Sofla, M. S. D. & Ashrafzadeh, A. 2021 Improving the performance of rainfall-runoff models using the gene expression programming approach. *Journal of Water and Climate Change* **12** (7), 3308–3329. https://doi.org/10.2166/wcc.2021.064.

Fang, Z., Wang, Y., Peng, L. & Hong, H. 2021 Predicting flood susceptibility using LSTM neural networks. *Journal of Hydrology* **594**, 125734. https://doi.org/10.1016/j.jhydrol.2020.125734.

Fleming, M. & Neary, V. 2004 Continuous hydrologic modeling study with the hydrologic modeling system. *Journal of Hydrologic Engineering* **9**, 175–183.

Garee, K., Chen, X., Bao, A., Wang, Y. & Meng, F. 2017 Hydrological modeling of the Upper Indus Basin: A case study from a high-altitude glacierized catchment Hunza. *Water* **9** (1), 17. https://doi.org/10.3390/w9010017.

Hamon, W. R. 1963 Computation of direct runoff amounts from storm rainfall. *International Association of Scientific Hydrology Publication* **63**, 52–62.

Hamdan, A. N. A., Almuktar, S. & Scholz, M. 2021 Rainfall-Runoff modeling using the HEC-HMS model for the Al-Adhaim River Catchment, Northern Iraq. *Hydrology* **8**, 58. https://doi.org/10.3390/hydrology8020058.

IPCC 2021 Climate change 2021: The physical science basis. In: *Contribution of Working Group I to the Sixth Assessment Report of the Intergovernmental Panel on Climate Change* (Masson-Delmotte, V., Zhai, P., Pirani, A., Connors, S. L., Péan, C., Berger, S., Caud, N., Chen, Y., Goldfarb, L., Gomis, M. I., Huang, M., Leitzell, K., Lonnoy, E., Matthews, J. B. R., Maycock, T. K., Waterfield, T., Yelekc, O., Yu, R. & Zhou, B., eds). Cambridge University Press, Cambridge, UK.

Kirpich, Z. 1940 Time of concentration of small agricultural watersheds. *Civil Engineering* **10**, 362.

Leavesley, G. H., Lichty, R. W., Troutman, B. M. & Saindon, L. G. 1983 *Precipitation-Runoff Modeling System; User's Manual. Water-Resources Investigations Report 83-4238*. https://doi.org/10.3133/wri834238.

Mohammadi, B., Safari, M. J. S. & Vazifehkhah, S. 2022 IHACRES, GR4J and MISD-based multi conceptual-machine learning approach for rainfall-runoff modeling. *Scientific Reports* **12**, 12096. https://doi.org/10.1038/s41598-022-16215-1.

Moradkhani, H. & Sorooshian, S. 2008 General review of rainfall-runoff modeling: Model calibration, data assimilation, and uncertainty analysis. In: *Hydrological Modeling and the Water Cycle. Water Science and Technology Library*, vol 63. (Sorooshian, S., Hsu, KL., Coppola, E., Tomassetti, B., Verdecchia, M. & Visconti, G., eds). Springer, Berlin, Heidelberg, p. 291.

Mosavi, A., Ozturk, P. & Chau, K.-w. 2018 Flood prediction using machine learning models: Literature review. *Water* **10**, 1536. https://doi.org/10.3390/w10111536.

Muralikrishna, I. V., Manickam, V., 2017 Chapter fourteen – air pollution control technologies. In: *Environmental Management* (Muralikrishna, Iyyanki V. & Manickam, Valli, eds). Butterworth-Heinemann, Oxford, pp. 337–397. https://doi.org/10.1016/B978-0-12-811989-1.00014-2.

Narayana Reddy, B. S. & Pramada, S. K. 2022 A hybrid artificial intelligence and semi-distributed model for runoff prediction. *Water Supply* **22** (7), 6181–6194. https://doi.org/10.2166/ws.2022.239.

Ni, L., Wang, D., Singh, V. P., Wu, J., Wang, Y., Tao, Y. & Zhang, J. 2020 Streamflow and rainfall forecasting by two long short-term memory-based models. *Journal of Hydrology* **583**, 124296. https://doi.org/10.1016/j.jhydrol.2019.124296.

Olah, C. 2015 *Understanding LSTM networks*. Retrieved November 12, 2018. Available from: http://colah.github.io/posts/2015-08-Understanding-LSTMs/.

Oleyiblo, J. O. & Li, Z. J. 2010 Application of HEC-HMS for flood forecasting in Misia and Wan'an catchments in China. *Water Science and Engineering* **3** (1), 14–22. https://doi.org/10.3882/j.issn.1674-2370.2010.01.002.

Ouédraogo, W. A. A., Raude, J. M. & Gathenya, J. M. 2018 Continuous modeling of the Mkurumudzi river catchment in Kenya using the HEC-HMS conceptual model: Calibration, validation, model performance evaluation and sensitivity analysis. *Hydrology* **5**, 44. https://doi.org/10.3390/hydrology5030044.

Prakasam, C., Saravanan, R., Machiwal, D. & Sharma, M. K. 2023 Rainfall-runoff modeling using HEC-HMS model in an ungauged Himalayan catchment of Himachal Pradesh, India. *Arabian Journal of Geosciences* **16**, 417 (2023). https://doi.org/10.1007/s12517-023-11519-6.

Rahman, K. U., Shang, S., Shahid, M. & Wen, Y. 2020 Hydrological evaluation of merged satellite precipitation datasets for streamflow simulation using SWAT: A case study of Potohar Plateau, Pakistan. *Journal of Hydrology* **587**, 125040. https://doi.org/10.1016/j.jhydrol.2020.125040.

Ren, Y., Zeng, S., Liu, J., Tang, Z., Hua, X., Li, Z., Song, J. & Xia, J. 2022 Mid- to long-term runoff prediction based on deep learning at different time scales in the Upper Yangtze River Basin. *Water* **14**, 1692. https://doi.org/10.3390/w1411169.

Sabol, G. V. 1988 Clark unit hydrograph and R-parameter estimation. *Journal of Hydraulic Engineering* **114** (1), 1. https://doi.org/10.1061/(ASCE)0733-9429(1988)114:1(1).

Saxton, K. E. & Willey, P. H. 2005 The SPAW model for agricultural field and pond hydrologic simulation. In: *Watershed Models* (Singh, V. P. & Frevert, D. K., eds). CRC Press, Boca Raton, FL, USA.

Shakarneh, M. O. A., Khan, A. J., Mahmood, Q., Khan, R., Shahzad, M. & Tahir, A. A. 2022 Modeling of rainfall–runoff events using HEC-HMS model in southern catchments of Jerusalem Desert-Palestine. *Arabian Journal of Geosciences* **15**, 127. https://doi.org/10.1007/s12517-021-09406-z.

Solgi, R., Loáiciga, H. A. & Kram, M. 2021 Long short-term memory neural network (LSTM-NN) for aquifer level time series forecasting using in-situ piezometric observations. *Journal of Hydrology* **601**, 126800. https://doi.org/10.1016/j.jhydrol.2021.126800.

Sorman, A. A., Tas, E. & Dogan, Y. O. 2020 Comparison of hydrological models in upper Aras Basin. *Pamukkale Üniversitesi Mühendislik Bilimleri Dergisi* **26** (6), 1015–1022.

Subramanya, K. 2008 *Engineering Hydrology*. Tata McGraw-Hill Publishing Company Limited, New Delhi.

Tasabat, S. & Aydın, O. 2021 Using long-short term memory networks with genetic algorithm to predict engine condition. *Gazi University Journal of Science* **35** (1). https://doi.org/10.35378/gujs.937169.

U.S. Army Corps of Engineers 2018 HEC-HMS User Manual (Version 4.4). Hydrologic Engineering Center. Available from: https://www.hec.usace.army.mil/software/hec-hms/documentation/HEC-HMS_Users_Manual.pdf.

Wen, S. & Feng, Z. 2023 Theoretical analysis and applications of artificial intelligence in hydrology and water resource management. *Water Supply* **23** (4), iii–ivi. https://doi.org/10.2166/ws.2023.080.

Xiang, Z., Yan, J. & Demir, I. 2020 A rainfall-runoff model with LSTM-based sequence-to-sequence learning. *Water Resources Research* **56**, e2019WR025326. https://doi.org/10.1029/2019WR025326.

Xiang, Y., Wang, Y., Chen, Y. & Zhang, Q. 2022 Impact of climate change on the hydrological regime of the Yarkant River Basin, China: An assessment using three SSP scenarios of CMIP6 GCMs. *Remote Sensing* **14**, 115. https://doi.org/10.3390/rs14010115.

Young, C.-C. & Liu, W.-C. 2015 Prediction and modeling of rainfall–runoff during typhoon events using a physically-based and artificial neural network hybrid model. *Hydrological Sciences Journal* **60** (12), 2102–2116. https://doi.org/10.1080/02626667.2014.959446.

Yu, X. & Zhang, J. 2023 The application and applicability of HEC-HMS model in flood simulation under the condition of river basin urbanization. *Water* **15** (12), 2249. https://doi.org/10.3390/w15122249.

First received 13 March 2024; accepted in revised form 1 July 2024. Available online 11 July 2024